PNAS RESEARCH ARTICLE | EVOLUTION

Dosage compensation and meiotic sex chromosome inactivation are maintained under relaxed selection

Darren J. Parker[a,b,1], Zoé Dumas[b], Rocío Gómez[c], Jean-Marc Aury[d], Marjorie Labedan[b], Patrick Tran Van[b], Benjamin Istace[d], Corinne Cruaud[e], Karine Labadie[e], Benjamin Noel[d], Susana Freitas[b], Jelisaveta Djordjevic[b], and Tanja Schwander[b,1]

Affiliations are included on p. 8.

Edited by Catherine L. Peichel, University of Bern, Bern, Switzerland; received November 4, 2025; accepted June 17, 2026

Dosage compensation and meiotic sex chromosome inactivation (MSCI) are key mechanisms regulating gene expression from the X chromosome in male-heterogametic species. While the convergent evolution of these mechanisms is well documented, their evolutionary fate under relaxed selection remains poorly understood. Here, we test whether dosage compensation and MSCI persist following three independent transitions to parthenogenesis in stick insects, where selection on male phenotypes is relaxed. Using rare males occasionally produced by parthenogenetic females, chromosome-level genome assemblies, RNA-seq from multiple tissues, and immunocytochemistry, we find that dosage compensation is fully conserved across all seven studied somatic tissues. This is even the case in the oldest, approximately 1.5 My old all-female lineage and for tissue-specific genes for which dosage variation is not expected to be very deleterious. Meiotic X inactivation in the germline is also conserved. Surprisingly, however, expression data and cytological markers indicate that MSCI signatures are even stronger in parthenogenetic males, a pattern likely driven by prolonged autosomal transcription during meiosis. These results indicate that X-targeting dosage compensation and MSCI are highly stable over evolutionary time and may be maintained in all-female lineages by a combination of evolutionary constraint, pleiotropy, or very weak selection, whereas autosomal expression during meiosis shifts rapidly under relaxed selection.

parthenogenesis | dosage compensation | meiotic sex chromosome inactivation

Significance

Sex chromosomes are regulated by specialized mechanisms that balance gene expression between the X chromosome and the autosomes in somatic tissues (dosage compensation) and silence the X chromosome during male meiosis (meiotic sex chromosome inactivation, MSCI). These processes are thought to decay when they become redundant, yet suitable systems to test this prediction are scarce. We studied rare males from parthenogenetic stick insect lineages that have been evolving without sex for up to 1.5 My. Surprisingly, both dosage compensation and MSCI remain fully functional, despite relaxed selection. Instead, we find altered autosomal expression during meiosis. Our results reveal that sex chromosome regulation is evolutionarily stable and constrained, persisting even after the loss of its purpose.

Sexual reproduction is key to the diversity of life and the main driver of species' lifecycles. In eukaryotic species with distinct male and female sexes, sex determination is frequently governed by sex chromosomes such as X and Y chromosomes in male heterogametic species (1). Because males carry only a single X chromosome while females carry two, X chromosome expression is regulated by highly specialized mechanisms: dosage compensation (in somatic cells) and meiotic sex chromosome inactivation (MSCI, in germ cells). Dosage compensation is a mechanism that balances the expression of X-linked and autosomal genes independently of the number of X chromosome copies. It has evolved independently across a wide range of taxa (2–4) including mammals (5), reptiles (6), fish (7, 8), nematodes (9), and insects (10–16). However, the X is typically not dosage compensated in gonads, where expression from the sex chromosome(s) is often further suppressed via MSCI (2, 12, 13, 17, 18). Specifically, MSCI involves the inactivation of heteromorphic sex chromosomes during meiosis through the addition of repressive chromatin marks, likely due to the inability of the X and the degraded (or completely lacking) Y to synapse at the onset of meiosis (19).

While far from ubiquitous (4, 20), dosage compensation and MSCI are typically maintained across clades for millions of years. Furthermore, a breadth of studies on both mechanisms indicate that they can evolve convergently as new sex chromosomes arise, involving similar or different mechanisms. This is revealed for example by research in dipterans, where X chromosomes have evolved independently from ancestral autosomes, with different dosage compensation mechanisms emerging in parallel (21–28). Similarly, the independent evolution of MSCI mechanisms in divergent taxa involves both shared and lineage-specific components (e.g., refs. 29–31).

In contrast to the evidence for the convergent de novo evolution of dosage compensation and MSCI, it remains unknown how ancestral dosage compensation and MSCI systems evolve once they become redundant, which would be the case upon the evolution of a novel sex chromosome system. This is in part because suitable model systems with sex chromosome turnovers and accompanying evolution of X-targeting regulatory mechanisms remain understudied. Furthermore, sex chromosome turnover events in species with established dosage compensation and MSCI systems are expected to be rare because the

Author contributions: D.J.P., Z.D., and T.S. designed research; D.J.P., Z.D., R.G., J.-M.A., M.L., P.T.V., B.I., C.C., K.L., B.N., S.F., and J.D. performed research; D.J.P., Z.D., R.G., J.-M.A., M.L., P.T.V., B.I., C.C., K.L., B.N., S.F., and J.D. analyzed data; and D.J.P. and T.S. wrote the paper.

The authors declare no competing interest.

This article is a PNAS Direct Submission.

[1]To whom correspondence may be addressed. Email: d.parker@bangor.ac.uk or tanja.schwander@unil.ch.

This article contains supporting information online at https://www.pnas.org/lookup/suppl/doi:10.1073/pnas.2531501123/-/DCSupplemental.

Published July 15, 2026.

maintenance of active systems could cause extensive misregulation of gene expression on the newly formed sex chromosomes (32–34). A unique opportunity to overcome such constraints is to study the fate and potential decay of dosage compensation and MSCI in all-female parthenogenetic species. Following a transition to parthenogenesis, the X chromosome effectively adopts an autosomal inheritance pattern as it no longer varies in copy numbers since all individuals are female and carry two X copies. As a result, if dosage compensation or MSCI is costly (because of the cost of the machinery or due to maladaptive expression in females) we would expect selection to reduce a species' ability to perform these mechanisms following a transition to parthenogenesis. In the absence of such costs in females, dosage compensation and MSCI would be expected to decay and vestigialize as a consequence of drift. A reduction of the two X regulatory mechanisms is difficult to observe in parthenogenetic species as we need to examine expression in both sexes. This barrier can be overcome in some systems if rare males are produced, a phenomenon frequently observed in parthenogenetic arthropods (35). The production of rare males would be impossible for species where the perturbation of dosage compensation is lethal in males, as is the case for certain mutations in the *Drosophila* fly dosage compensation machinery (e.g., ref. 36). However, the suppression of dosage compensation does not affect male viability in *Anopheles* mosquitoes and instead causes a developmental delay (25). This variation between taxa illustrates that inference regarding the functioning and maintenance of dosage compensation cannot be based on the observation of male phenotypes in parthenogenetic species. With respect to X regulation in the germline, X-autosome translocations negatively affect fertility in *Drosophila* flies (37, 38), where X regulation happens via a mechanism that differs from classical MSCI as described in mammals and other insect taxa (17, 39). For other insects, fertility consequences of MSCI perturbation are unknown. As a consequence, fertility or sperm viability phenotypes in rare males do not provide information about the functioning of MSCI. More broadly, the production of rare but fertile males implies that many male-specific developmental and reproductive functions remain intact after the transition to parthenogenesis. This is consistent with very slow decay of male traits under relaxed selection (35).

Here, we take advantage of such rare males to examine dosage compensation and MSCI in three species of parthenogenetic *Timema* stick insects, using a combination of new chromosome-level genome assemblies, RNA sequencing of eight different tissues, and cell biology. *Timema* have had multiple independent transitions to parthenogenetic reproduction over the last 0.5 to 1.5 My (40–43). Previously, we have found that sexual *Timema* species show complete dosage compensation in somatic tissues throughout development, and MSCI in the male germline (11, 17, 44). This targeted regulation of the X chromosome likely involves general molecular mechanisms shared across insects (17) given that the stick insect X chromosome likely evolved prior to the diversification of insects over 450 Mya (33). We can examine changes in dosage compensation and MSCI in parthenogenetic *Timema* as they occasionally produce rare males via two different processes. Some males arise from aneuploidy of the X chromosome (45), which since *Timema* have an XX/X0 sex-determination system, results in the production of a male. Others develop as a consequence of very rare instances of sex within parthenogenetic populations (46). Field and experimental evidence indicates that males produced by parthenogenetic *Timema* are exceedingly rare and exhibit reduced reproductive performance (45). During extensive field collections conducted over multiple years (2007–2012), only 11 males were recovered across several independently derived parthenogenetic lineages, despite the simultaneous collection of very large numbers of females. Functional assays of sperm performance further demonstrate that while rare males are capable of fertilization when mated as the sole partner of virgin females from closely related sexual species, reproductive success is low and they fail entirely under sperm competition (45). Thus, male production in parthenogenetic *Timema* is both extremely infrequent and associated with reduced reproductive performance. These features indicate relaxed selection on male-specific traits, while still allowing the occasional availability of males for mechanistic analyses of dosage compensation and MSCI. Contrary to our expectations we find that the targeted regulation of the X chromosome underlying dosage compensation and MSCI has been fully conserved in each of the three parthenogenetic lineages, with relaxed selection affecting autosomal rather than X-linked expression in male meiotic cells. These results indicate that selection against X-regulatory mechanisms is weak or that changes to dosage compensation and MSCI mechanisms are highly constrained.

Results and Discussion

Genome Assemblies Reveal a Highly Conserved X Chromosome Contrasted by Autosomal Fissions and Fusions. We generated chromosome-level genome assemblies for two of the three sexual species of *Timema* used in this study, *Timema cristinae* and *Timema podura*, to complement the available assembly of *Timema poppense* (*SI Appendix*, Table S1). In both new assemblies, the number of large scaffolds assembled (hereafter referred to as chromosomes) matched previous karyotype information (40) and coverage of male- vs. female-derived short reads were used to identify the X chromosome (*SI Appendix*). Annotation using a combination of gene predictions, protein, and RNAseq evidence from each species and its parthenogenetic sister species and inference of 8,118 one-to-one orthologs (*Methods*) revealed that the X chromosome content has not changed in any of the sexual or parthenogenetic species, as expected given the long-term conservation of X chromosome content in stick insects (11, 47). Using comparisons with a stick insect (*Bacillus rossius*) from the Euphasmatodea clade (which split over 120 Mya from *Timema* (48), we further find that even X chromosome synteny is highly conserved, while many rearrangements are apparent on the autosomes (Fig. 1). Specifically, the change in karyotype from 14 to 12 chromosomes during *Timema* evolution (40) involved at least two fissions and three fusions involving *T. podura* chromosomes 2, 3, 5, and 10 (Fig. 1 and *SI Appendix*, Fig. S1).

Dosage Compensation in Somatic Tissues Is Not Reduced in Parthenogenetic Species. Dosage compensation between the sexes in parthenogenetic species was very similar to that observed in sexual species. In all seven nonreproductive tissues (antennae, brain, defense glands, gut, fat body, femur, and tarsi) we observe almost complete dosage compensation in all species (Fig. 2). As expected, we observe some variation in the expression of X-linked genes between the sexes for specific tissues and species (resulting in small but significant differences in expression of autosomal vs. X-linked genes). Such variation is typical in studies of dosage compensation (e.g., refs. 13, 49, and 50) and can be interpreted as sex-specific regulation of individual genes rather than a consequence of variable or incomplete dosage compensation. If dosage compensation was reduced in parthenogenetic species, we would expect to see a larger deviation from complete dosage compensation in parthenogenetic species and an accompanying lower male-to-female expression ratio for the X in parthenogenetic

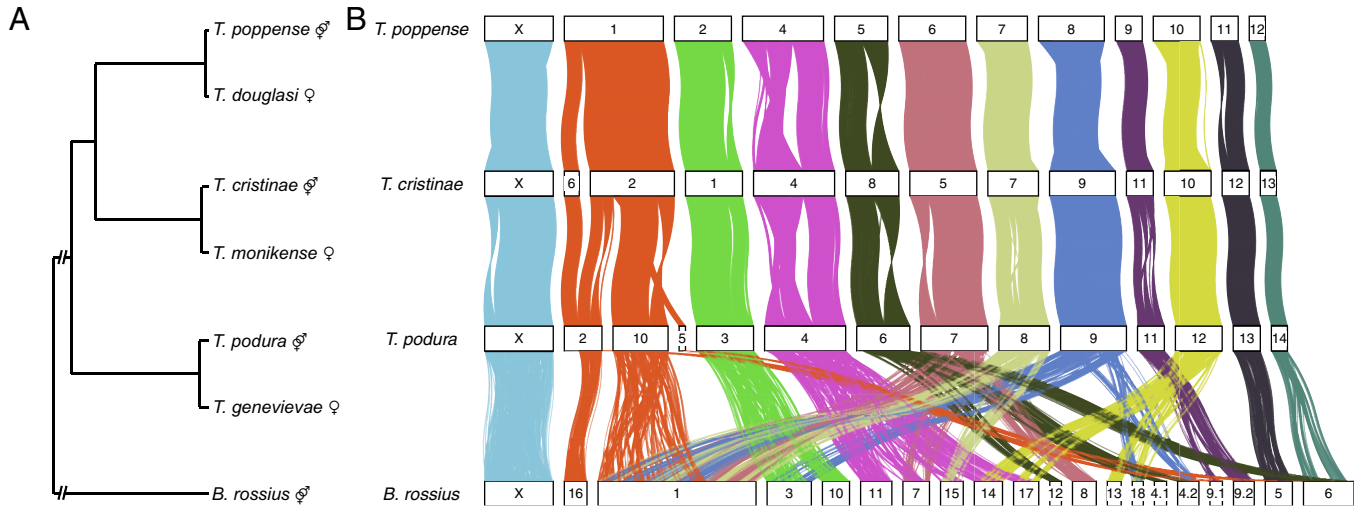

Fig. 1. Autosomal genomic instability contrasts with X chromosome conservation. (*A*) Simplified phylogeny of the used species, highlighting the independently evolved parthenogenetic *Timema* species and their closest sexual relatives. *Timema* are the sister clade to all other stick insects (including *B. rossius*), and branches reflecting this split have been shortened for display. (*B*) Chord diagram showing synteny between the assemblies of sexual species, based on 4,241 one-to-one orthologs across the focal *Timema* genomes and a distantly related stick insect (*B. rossius*). See *SI Appendix*, Fig. S1 for synteny based on 8,118 one-to-one orthologs across *Timema* only, for a better resolution of detected rearrangements within the *Timema* genus.

species when compared to the sexual sister species for tissues with almost complete dosage compensation. We do not observe this, instead finding only small variations in X-linked expression with no consistent pattern (Fig. 2 and *SI Appendix*, Figs. S2–S14 and Table S2), showing that dosage compensation is maintained across tissues even under relaxed selection for up to 1.5 My. This conclusion extends to more in depth analyses: The amount of dosage compensation is consistent between the sexual and parthenogenetic species on a gene-by-gene basis (*SI Appendix*, Figs. S2–S7), and we also find no evidence for decreased efficiency of dosage compensation for genes with tissue-specific expression (*SI Appendix*, Figs. S8–S10), which are expected to be relatively less constrained than housekeeping genes (51).

Parthenogenetic species no longer require sex-specific regulation of the X chromosome. Under such conditions, the strength of selection acting on dosage compensation mechanisms is expected to be substantially reduced. Whether this relaxation should lead to detectable evolutionary decay depends on several unknown parameters, including the number of loci involved, mutational target size, and the degree of pleiotropy. If the machinery is costly or maladaptive in females, selection could favor its reduction. Alternatively, if costs are negligible, its evolution would be governed largely by drift. The absence of detectable change over up to 1.5 My therefore indicates either unusually slow neutral decay, functional constraint, or the action of weak purifying selection, but does not allow us to distinguish conclusively among these alternatives. Any contribution of weak purifying selection is likely to be minimal. Although selection acting on rare males could, in principle, maintain dosage compensation, the extreme rarity and reduced fertility of these males (45) imply that such selection would be very weak. A better case can be made for the potential involvement of functional constraints due to pleiotropic effects in females from evidence for the maintenance of dosage compensation-like mechanisms targeting the ancestral X in *Drosophila melanogaster* fruit flies (52). A sex chromosome turnover reverted the ancestral X (now referred to as the dot) back to an autosome in the *Drosophila* lineage (15). Similar to our present study in parthenogenetic species, such reversals should result in relaxed selection for dosage compensation on the ancestral X (dot) chromosome. Yet, the dot still features chromosome-specific regulatory factors, including a protein called *Painting of fourth* (POF) (52). Interestingly, POF is part of the dosage compensation machinery in the sheep blow fly *Lucilla* [where the POF ortholog is called "*no blokes*," or *nbl* (27)]. Thus, in *Drosophila*, the regulation of the dot via POF might reflect vestiges of the former dosage compensation machinery when the dot was still the X chromosome.

A second reason to expect changes in dosage compensation could be if dosage compensation mechanisms result in maladaptive gene expression in females, i.e., partially unresolved sexual antagonism (53). This factor may not have a strong influence in *Timema* as unresolved antagonisms are expected to be transient (54) and the stick insect X chromosome is very old and highly conserved (Fig. 1) and shares content with the X chromosome in other insect orders that diverged over 450 Mya (33). Any maladaptive gene expression in females as a result of sexual conflict over dosage compensation would therefore be expected to be very small.

While our results show that dosage compensation is maintained in parthenogenetic species because selection in females against dosage compensation components is weak or because changes to the underlying mechanisms are constrained, we cannot exclude that perhaps not enough time has passed since the evolution of parthenogenesis to observe any changes to dosage compensation. Particularly under a fully neutral-drift scenario, timescales to observe decay could be longer for complex regulatory systems such as dosage compensation and MSCI (55, 56). Similarly, under a selective scenario (where there is selection against male-essential components of dosage compensation in females) a lack of time may be a plausible explanation in the young lineage *T. douglasi* and for the lack of apparent changes in dosage compensation in whole-body samples of males of parthenogenetic aphid lineages (57), however, it is very unlikely for the oldest species used here (*T. genevievae*) with an age estimate of over 1.5 My (41, 42, 55).

A Stronger Signature of MSCI in Parthenogenetic than Sexual Species Driven by Autosomal Misexpression during Meiosis. We have shown previously that the X chromosome is consistently inactivated throughout male meiosis in sexual *Timema* species (17, 44). Accordingly, we observe very low expression of X-linked genes in the testes, much lower than the expectation for a lack of dosage compensation (Fig. 3 and *SI Appendix*, Figs. S15 and S16

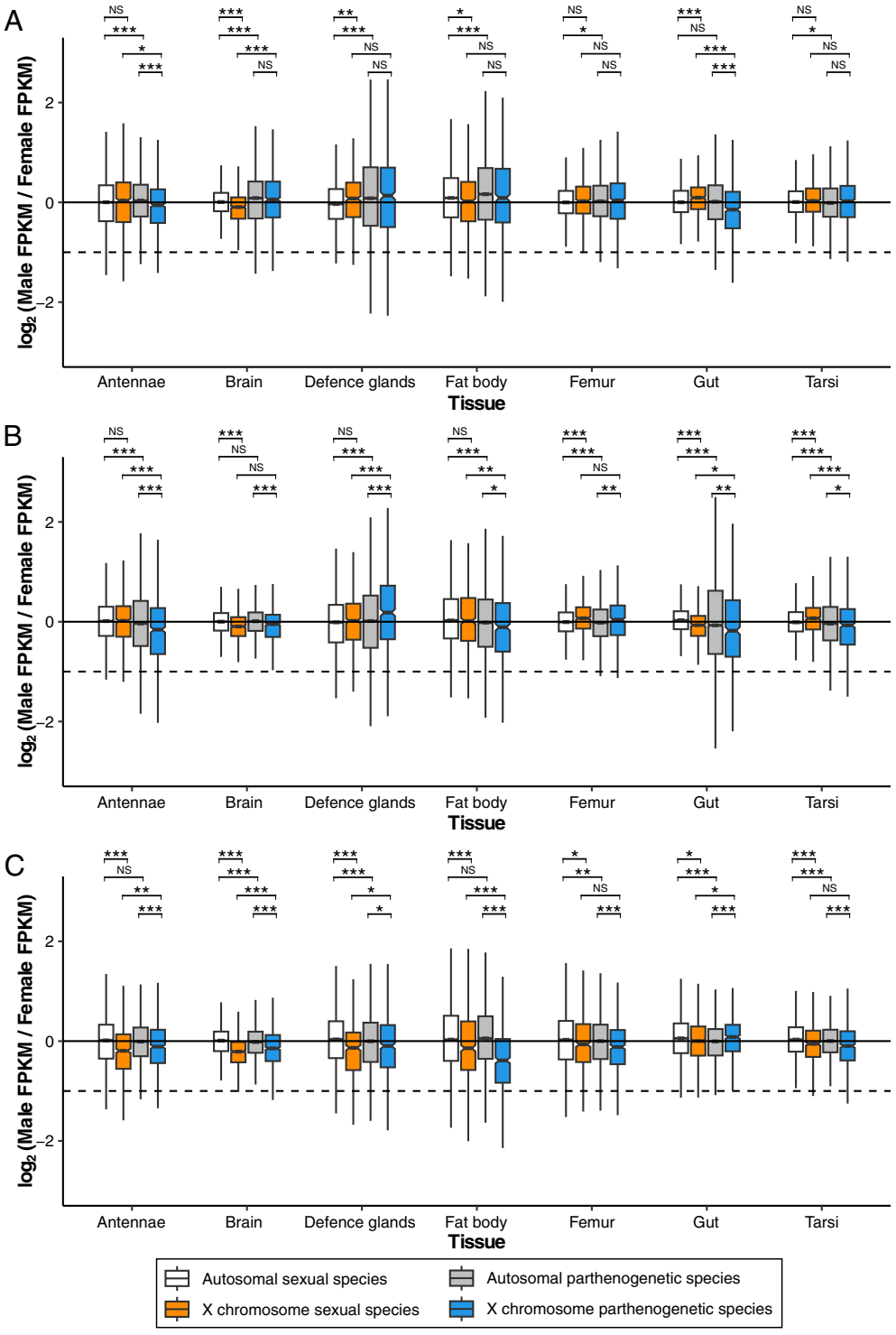

Fig. 2. Male to female expression ratios for the X and autosomes in nonreproductive tissues reveal the maintenance of dosage compensation under relaxed selection. Dashed lines represent a twofold reduction in expression in males (as expected if there was no dosage compensation). (*A*) Sexual species = *T. cristinae*, parthenogenetic species = *Timema monikense*. (*B*) Sexual species = *T. podura*, parthenogenetic species = *Timema genevievae.* (*C*) Sexual species = *T. poppense*, parthenogenetic species = *Timema douglasi.* Asterisks indicate the significance (FDR) of Wilcoxon tests (***< 0.001, **< 0.01, *< 0.05, NS > 0.05).

and Table S3). We do however still observe some expression of the X in males, as expected given the presence of nonmeiotic cells in testes. Surprisingly, we see a consistently lower expression of X-linked genes in males from parthenogenetic than sexual species (Fig. 3 and *SI Appendix*, Figs. S15 and S16). This could indicate variable cellular composition of testes such as a higher proportion of meiotic cells (and thus a higher number of cells with inactivated X chromosomes) in parthenogenetic than sexual males, or, more likely (see below), that autosomal expression is more persistent across meiosis in parthenogenetic as compared to sexual males. RNA-seq expression estimates are inherently relative rather than absolute measures. In our dataset, normalization is dominated by autosomal genes because they constitute the majority of expressed loci. As a result, increased autosomal transcription during meiosis can make X-linked expression appear relatively lower after normalization, even if absolute X-linked transcription has not changed. Therefore, the stronger MSCI signature in parthenogenetic males could reflect either reduced X expression

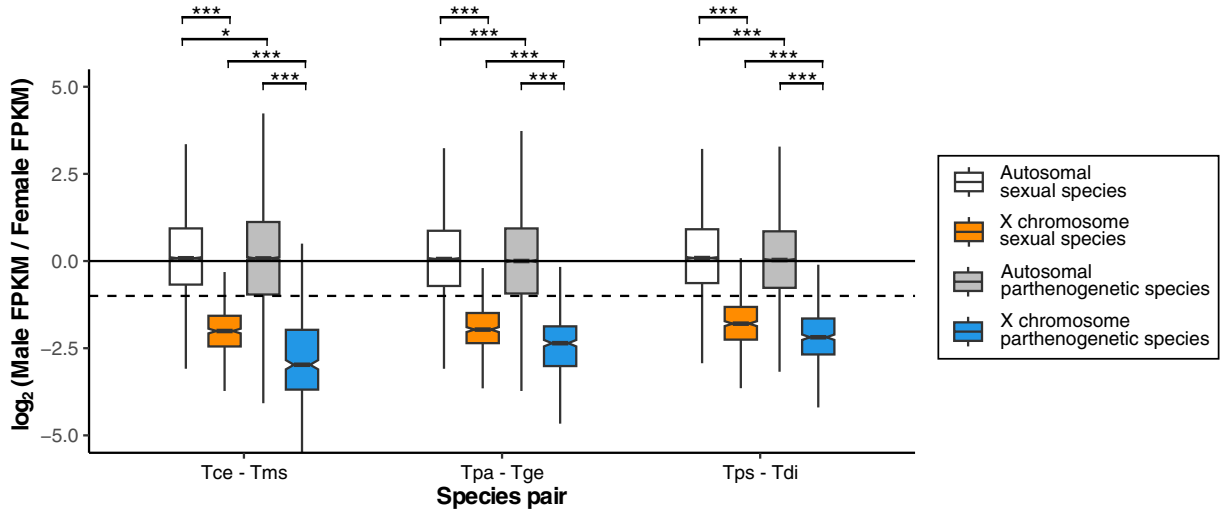

Fig. 3. A stronger signature of MSCI in parthenogenetic than sexual species. Gene expression in reproductive tissues: Log_2 of male to female expression ratio for the X and autosomes in testes and female gonads. Species codes: Tce = *T. cristinae*, Tms = *T. monikense*, Tpa = *T. podura,* Tge = *T. genevievae,* Tps = *T. poppense,* Tdi = *T. douglasi.* Asterisks indicate the significance (FDR) of Wilcoxon tests (***< 0.001, **< 0.01, *< 0.05, NS > 0.05). Dashed lines represent a twofold reduction in expression in males (as expected if there was no dosage compensation). Positive values indicate higher expression in males than females, while negative values indicate lower expression in males.

or increased autosomal expression; however, these data do not allow these alternatives to be fully separated.

In sexual *Timema* males, there are two bursts of autosomal transcription during meiosis [(44); Fig. 4] a first at the end of prophase I (specifically, during pachytene and diplotene stages), and a second during meiosis II at the spermatid stage. To detect potential changes to these temporal patterns of autosomal expression in parthenogenetic males, we performed immunolabeling of testis tissue of *T. monikense* and *T. douglasi* using RNA polymerase II, a conserved transcriptional marker. For comparison, we used the previously characterized expression pattern from the sexual species *T. californicum* (44), a sexual *Timema* species that is a closely related outgroup to the *T. poppense*–*T. douglasi* species pair. This labeling revealed that autosomal expression during prophase I is longer in parthenogenetic than sexual males. In the former, the RNA polymerase II signal already appears at the onset of prophase I (i.e., during the zygotene stage; Fig. 4 and *SI Appendix*, Fig. S17) and is maintained until diplotene (Fig. 4 and *SI Appendix*, Fig. S17), while in the latter it only appears at pachytene (44) (Fig. 4). Since males of parthenogenetic species are not exposed to selection, this extension of the autosomal transcription burst during prophase I is most likely a consequence of drift, i.e., it reflects autosomal misexpression during meiosis in parthenogenetic males. Importantly, the RNA polymerase II immunolabeling supports the interpretation that autosomal transcription persists for longer during meiosis in parthenogenetic than sexual males. This is most consistent with a relative increase in autosomal expression rather than a decrease in X-linked expression underlying the stronger signature of MSCI in parthenogens (Fig. 3).

Conclusion

Our results demonstrate that both dosage compensation and MSCI are robustly maintained in parthenogenetic stick insects, despite the long-term absence of selective pressures typically associated with male phenotypes. This maintenance suggests that the molecular mechanisms underlying dosage compensation and MSCI are either functionally constrained (e.g., due to pleiotropic effects in females), maintained by weak purifying selection (for example through sufficiently frequent reproduction of rare males), or decay too slowly as a consequence of drift for phenotypic effects to be observed in the stick insects. Nevertheless, the enhanced signature of MSCI in parthenogenetic males appears to be driven by extended autosomal transcription during meiosis, revealing an unexpected consequence of relaxed selection on gene expression. Together, these findings highlight the stability and evolutionary inertia of complex regulatory processes, even in the face of dramatic shifts in reproductive mode.

Methods

Reference Genome Assemblies. Reference genome assemblies were produced for *T. cristinae* (Bioproject PRJNA1268975/Accession JBOIUC000000000) and *T. podura* (Bioproject PRJNA1268975/Accession JBOIUD000000000) from wild collected females (GPS coordinates 34°30′53.2″N, 119°46′45.3″W and 33°47′47.0″N, 116°46′34.6″W). Contigs for the *T. cristinae* assembly were based on PacBio sequencing (43×) and on a combination of Nanopore and Illumina sequencing for *T. podura* (sequenced at 85× respectively 62× coverage). Scaffolding was done using a Hi-C library (sequenced at approximately 69× and 53× coverage for *T. cristinae* and *T. podura* respectively) to produce the final reference assembly.

DNA Extraction and Library Preparation. To extract high molecular weight (HMW) DNA, we flash-froze a single female (without gut) in liquid nitrogen and ground it using a Cryomill (Retsch). We then extracted HMW DNA using a G/20 Genomic Tips kit (Qiagen) following the manufacturer's protocols and checked DNA integrity on a pulse field agarose gel.

For *T. cristinae*, a PacBio library was prepared using the Template Prep Kit 1.0 following the manufacturer's instructions and sequenced on a single cell of the PacBio SMRT™ system. For *T. podura*, four ONT libraries were prepared following Oxford Nanopore instructions. A first library was prepared using the SQK-LSK108 ligation sequencing kit and was loaded on a MinION R9.4 Flow Cells, and then three libraries were prepared using the SQK-LSK109 ligation sequencing kit and were loaded on three PromethION R9.4.1 Flow Cells. A PCR free Illumina library (based on the same HMW extraction) was prepared using the Kapa Hyper Prep Kit (Roche, Basel, Switzerland), following manufacturer instructions. The library was quantified by qPCR using the KAPA Library Quantification Kit for Illumina Libraries (Roche), and the library profile was assessed using a High Sensitivity DNA kit on an Agilent Bioanalyzer (Agilent Technologies, Santa Clara, CA, United States). The library was then sequenced on an Illumina HiSeq 4000 instrument (Illumina, San Diego, CA, United States), using 150 base-length read chemistry in a paired-end mode.

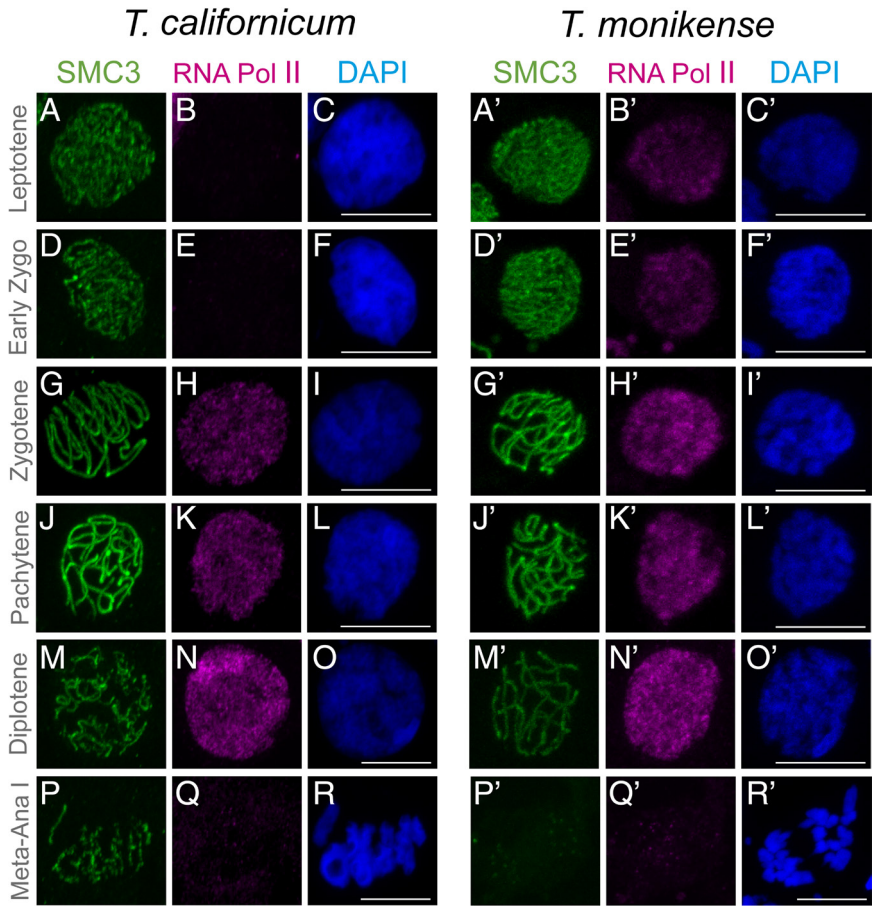

Fig. 4. Misregulation of autosomal gene expression in meiotic cells of rare males produced by parthenogenetic females. RNApol-II distribution in meiocytes of sexual (*T. californicum*) and parthenogenetically produced (*T. monikensis*) males. The pattern observed in *T. californicum* was reported previously (44) and is included here as a sexual reference to facilitate comparison with the parthenogenetic males. Projections of stack images acquired across squashed meiocytes at the stages indicated, stained with DAPI (blue) and double immunolabeled for SMC3 (green) and RNApol-II (magenta). RNApol-II labeling is already present at leptotene and early zygotene in parthenogenetic *T. monikensis* males, while it only appears during late zygotene in sexual *T. californicum* males, as shown previously (44). Note that the used immunolabeling allows for inference of qualitative (presence–absence) rather than quantitative (intensity of signals) differences. (Scale bar, 10 μm.) Corresponding image analyses for males of *T. douglasi* are available in *SI Appendix*, Fig. S17.

A Hi-C library was prepared for each species using the Proximo Hi-C Kit. We generated ground tissue for cross-linking using Cryomill (Retsch) and following manufacturer instructions, using a different female than the one used for Nanopore and HiSeq sequencing, from the same natural population. Library construction and sequencing (250 million read pairs) was outsourced to Phase Genomics (Seattle).

Assembly Pipelines. We used different strategies for genome assembly for the two species. For *T. cristinae* raw PacBio reads were assembled into contigs using Canu (58) with the parameter correctedErrorRate = 0.105. For *T. podura* raw Oxford Nanopore reads were filtered using Filtlong v0.2.0 (https://github.com/rrwick/Filtlong) with the parameters --min_length 1000 --keep_percent 90 --target_bases 69050000000. The filtered Nanopore reads were then assembled into contigs using Flye v2.8.1 (59) with --genome-size 1.381 g. All Nanopore reads were mapped against the contigs using minimap2 v2.19 (60) with the parameters -c -x map-ont and a first step of polishing was performed using Racon v1.4.3 (61). Three additional rounds of polishing were conducted: Illumina short reads were aligned to the contigs using BWA mem v0.7.17 (62) and polishing was performed using Pilon v1.23 (63).

Both assemblies were then decontaminated using BlobTools v1.0 (64) under the taxrule "bestsumorder." Hit files were generated after a blastn v2.10.1+ against the NBCI nt database, searching for hits with an e-value below 1e-25 (parameters: -max_target_seqs 10 -max_hsps 1 -evalue 1e-25). Contigs without hits to metazoans were removed from the assemblies. Haplotypic duplications were then filtered out as follows. Filtered reads were then mapped against the decontaminated genomes using minimap2 and haplotigs were detected with Purge Haplotigs v1.1.1 (65) using the parameters -l 3 -m 27 -h 190 -j 101 --editor-coarse-resolution 250,000 for *T. cristinae* and -l 3 -m 45 -h 195 -j 101 --editor-coarse-resolution 50,000 for *T. podura*.

Hi-C reads from each species were then mapped against their respective haploid genome using Juicer v1.6 (66) with the restriction site Sau3AI. Finally, chromosome-level scaffolding was performed using 3D-DNA v180922 (67) with species-specific parameters, as recommended by the authors. The resulting Hi-C contact matrices were visualized with Juicebox, and minor polishing was conducted in accordance with these recommendations. The completeness of both genome assemblies was assessed with BUSCO v5.1.2 (68) against the *insecta_odb10* dataset using the --long and --augustus parameters.

Annotation. We annotated the *T. cristinae* and *T. podura* genomes in a similar way as we previously annotated the *T. poppense* genome (17), using a combination of ab initio gene prediction, protein homology, and RNA-seq using the Braker2 pipeline (v. 2.1.6) (69). First, each genome assembly was soft-masked using RepeatModeler (v. 2.0.2, options: -LTRStruct, -engine ncbi) (70) and RepeatMasker (v. 4.1.2, options: -engine ncbi, -xsmall) (71). For protein evidence, we used the arthropod protein sequences from OrthoDB (v.10.1) (72) and the predicted protein sequences for *Timema* from our previous genome assemblies. For RNAseq evidence, we used the RNAseq libraries generated here for *T. cristinae* and *T. monikense* along with publicly available data {163 libraries generated here, 43 public [Bioproject accessions: PRJNA380865, PRJNA679785, PRJNA1295360, and PRJNA504764 (42, 43, 73)]} to annotate the *T. cristinae* genome and for *T. podura* and *T. genevievae* {119 libraries generated here, 29 public [Bioproject accessions: PRJNA380865, PRJNA679785, and PRJNA1295360 (42, 43)]} to annotate the *T. podura* genome. This is a total of 354 RNAseq libraries (330 paired-end, 24 single-end) covering over 19 different life stages, tissue, and sex combinations for each species (*SI Appendix*, Table S4). Reads

were quality trimmed with Trimmomatic (v. 0.39, options: ILLUMINACLIP:3:25:6 LEADING:9 TRAILING:9 SLIDINGWINDOW:4:15 MINLEN:80) (74) before mapping to the genome assembly with STAR (v. 2.7.8a, options: --twopassMode Basic) (75). Braker2 was run using protein evidence and RNAseq separately with the gene predictors Augustus (v. 3.4.0) (76) and Genemark (v. 4.72) (77). Following the RNAseq run, UTR predictions were added to the RNAseq gene predictions using GUSHR (v. 1.0) in Braker2 (--addUTR = on). The separate gene predictions were then merged using TSEBRA (v1.0.3) using the pref_braker1.cfg configuration file, which weights RNAseq evidence more strongly than the default option. We then ran BUSCO (v. 5.3.2, insecta_odb10) on the gene regions annotated by Braker2 and on the whole genome assembly. Any genes found by BUSCO but missed by Braker were then added to the annotation (69 genes for *T. cristinae* and 19 genes for *T. podura*). ncRNA genes were predicted using Infernal (v. 1.1.2, minimum e-value 1e-10) (78). GO-terms for protein-coding gene predictions were obtained using blastP within OmicsBox (v3.1.2, default parameters) to blast the nr *D. melanogaster* database (taxonomy filter: 7227). 1-to-1 orthologs between were obtained for protein-coding genes using OrthoFinder (version 2.5.5) (79) with default options.

Identification of the X chromosome. We used a coverage approach to identify X-linked scaffolds in our new genome assemblies. To do this we mapped publicly available Illumina genome reads from males and females [four males and five females for *T. cristinae* and four males and two females for *T. podura* PRJNA670663 and PRJNA725673 (11, 43)] to the respective genome assemblies and their publicly available mtDNA genomes using BWA-MEM (v. 0.7.15). Multimapping and poor quality alignments were filtered (removing reads with XA:Z or SA:Z tags or a mapq <30). PCR duplicates were removed with Picard (v.2.9.0) (http://broadinstitute.github.io/picard/). Coverage was then estimated for 100,000 bp sliding windows using BEDTools (v.2.26.0) (80). To compare coverage between males and females, coverage was first summed for all male and all female libraries per window. Male and female coverage was then normalized by modal coverage to adjust for differences in overall coverage. X- linked windows were then identified using the $\log_2$ ratio of male to female coverage. Autosomal windows should have equal coverage in males and females ($\log_2$ ratio of male to female coverage ≈ 0) and X-linked windows should have half the coverage in males as in females ($\log_2$ ratio of male to female coverage ≈ -1). This approach identified one large scaffold in each assembly as the X chromosome (*SI Appendix*, Figs. S18–S20).

We then repeated these analyses using genome reads from each of the parthenogenetic species. Female reads were publicly available [five for *T. monikense*, six for *T. genevievae*, and five for *T. douglasi*, PRJNA670663 (43)] as were the two male samples for *T. douglasi* [PRJNA808673, (81)]. For *T. monikense* and *T. genevievae* we also generated new Illumina libraries for males [two for *T. genevievae* and four for *T. monikense*) and an additional female library for *T. genevievae* (Accession number: PRJNA1293928) as described previously (43) using the carcasses after tissue dissection described below. Reads were then mapped to the genome of each sexual sister species as described above [the sexual species genome for *T. douglasi* is our previously published genome *T. poppense,* Accession number: PRJNA1126215 (17)]. Each of the newly generated samples were checked for normal coverage distributions before calculating coverage ratios.

RNA Extraction and Sequencing. We generated a total of 282 RNA-seq libraries for eight female tissues (antennae, brain, defense glands, fat body, femur, tarsi, and gonads) and nine male tissues (the same as the female plus the male accessory glands) for *T. cristinae*, *T. podura*, *T. monikense*, and *T. genevievae* following our previously developed methodology (17) (*SI Appendix*, Table S4). Individuals were collected as nymphs in the field and reared to adulthood in the laboratory. Prior to dissection all individuals were isolated in Petri dishes and fed on an artificial diet (a mix of flour, sugar, and water) for 2 d, allowing their gut contents to be cleared of plant material. Insects were then anesthetized with CO_2, dissected, and tissues individually flash-frozen in liquid nitrogen before being stored at −80 °C.

TRIzol solution (1 mL) and a small amount of ceramic beads (Sigmund Lindner) were added to each tissue. Samples were homogenized using a tissue homogenizer (Precellys Evolution; Bertin Technologies). Chloroform (200 µL) was added to each sample and samples were then vortexed for 15 s and centrifuged for 25 min at 12,000 rpm at 4 °C. The upper phase containing the RNA was then transferred to a new 1.5 mL tube with the addition of isopropanol (650 µL). The samples were vortexed and placed at −20 °C overnight. Samples were then centrifuged for 30 min at 12,000 rpm at 4 °C. The liquid supernatants were removed, and the RNA pellet underwent two washes using 80% and 70% ethanol. Each wash was followed by a 5-min centrifugation step at 12,000 rpm. Finally, the RNA pellet was resuspended in nuclease-free water and quantified using a fluorescent RNA-binding dye (QuantiFluor RNA System) and nanodrop (DS-11 FX).

Library preparation using NEBNext (New England BioLabs) and sequencing on an Illumina NovaSeq 6000 platform with 100 bp paired-end sequencing (36.2 million read pairs per sample on average) was outsourced to a sequencing facility (Fasteris, Geneva).

Gene Expression Analyses. We mapped RNAseq reads from *T. cristinae*, *T. podura*, *T. monikense*, and *T. genevievae* generated here and reads for *T. poppense* and *T. douglasi* we generated previously (17) to their respective sexual species genomes as described above. This gave four replicates for each of the 16 sex and tissue combinations for each of the six species, except for the male samples of parthenogenetic species (*T. monikense, T. genevievae,* and *T. douglasi*) where we had fewer replicates due to the difficulty of obtaining these specimens (n = 2 to 4; *SI Appendix*, Table S5). Read counts were obtained using HTSeq v.0.9.1 (82), with the following options (htseq-count --order = name --type = exon --idattr = gene_id --stranded = reverse). Expression analyses were performed using the Bioconductor package EdgeR (v 3.42.4) (83), and done separately for each species and tissue. Normalization factors for each library were computed using the TMM method and were used to calculate normalized expression levels (FPKM, Fragments Per Kilobase of transcript per Million mapped reads). mtDNA, rRNA, tRNA, and genes with low expression (less than 2 FPKM in 2 or more libraries per sex in either the sexual or parthenogenetic sister species) were excluded. This filtering was done to ensure that genes used for gene expression comparisons between sexual and parthenogenetic sister species and between males and females were the same. To examine dosage compensation, we used the $\log_2$ ratio of mean male expression level to female expression level and used Wilcoxon tests [adjusted for multiple testing using Benjamini and Hochberg's (84) algorithm] to determine if differences in expression between the autosomes and the X chromosome were significant.

Immunolabeling of Parthenogenetic Male Meiotic Cells. In order to determine the dynamics of autosomal gene expression during meiosis in parthenogenetic males, we followed the same protocol previously used to characterize autosomal gene expression during meiosis in sexual males (44). In brief, we performed double immunolabeling of SMC3_488 (#AB201542, AbCam) as a marker of cohesin axes (this allows for the assessment of synapsis progression, and hence, cell cycle stage) and RNA polymerase II phosphorylated at serine 2 (p-RNApol-II (ab193468, AbCam); an indicator of transcription). Gonads from adult *T. monikense* and *T. douglasi* males were dissected in 1× PBS, then fixed in paraformaldehyde (2%) and Triton X-100 (0.1%) solution for 15 min. Gonads were then squashed on slides coated with poly-L-lysine, and flash frozen in liquid nitrogen. Slides were incubated in PBS 1× for 20 min at room temperature, then blocked with a BSA 3% solution (prepared by dissolving 3 g of BSA in 100 mL of PBS 1×) for 20 min. Slides were then incubated overnight at 4 °C in a humid chamber with the primary (p-RNA-Pol II), diluted in BSA 3% (1:100), and washed 3× for 5 min in PBS 1×. The secondary antibody, anti-rabbit Alexa 594 (711-585-152, Jackson), diluted in BSA 3% (1:100), was applied, and samples were incubated for 45 min at room temperature. Further washes were conducted as described above, followed by an extended 10-min wash in PBS 1×, and by blocking using a 5% Normal Rabbit Serum (NRS) solution (X090210-8, Agilent Technology) for 30 min at room temperature. Another 5-min wash in PBS 1× was performed to remove excess blocking solution. Samples were then incubated with the labeled antibody SMC3_488 (#AB201542, AbCam) at a 1:100 dilution for 1 h at room temperature, followed by a final series of washes and staining with DAPI (D9542, Sigma-Aldrich) for 3 min at room temperature. Finally, after a 5-min wash in 1× PBS, two drops of Vectashield were added to the slide, which was then covered with a coverslip, and sealed with nail varnish for imaging. Image acquisition was performed at the Cellular Imaging Facility (CIF, University of Lausanne) using a Zeiss LSM 880 Airyscan.

Data, Materials, and Software Availability. Sequencing data have been deposited in SRA Genome assemblies have been deposited at DDBJ/ENA/GenBank under the accessions JBOIUC000000000 (*T. cristinae*) (85) and JBOIUD000000000 (*T. podura*) (86). The Illumina and PromethION sequencing data for *T. podura* are available in the European Nucleotide Archive under the following project PRJEB94285 (87). Male genomic reads have been deposited

at SRA under the following project PRJNA1293928 (88). RNAseq reads have been deposited at SRA under the following projects: PRJNA1320679 (89) and PRJNA1327219 (90). Code and annotations are available here: https://github.com/DarrenJParker/Timema_DC_MSCI_code (91) and will be archived upon acceptance. All other data are included in the manuscript and/or *SI Appendix*.

ACKNOWLEDGMENTS. This work was supported by the European Research Council Consolidator Grant 864672 ("No Sex No Conflict," T.S.), Swiss National Science Foundation Grant 31003A_182495 (T.S.), the Genoscope, the Commissariat à l'Énergie Atomique et aux Énergies Alternatives, and France Génomique (ANR-10-INBS-09–08). We thank the Lausanne Genomic Technologies Facility for PacBio library preparation and sequencing.

Author affiliations: [a]Molecular Ecology and Evolution Group, School of Natural and Environmental Sciences, Bangor University, Bangor LL57 2UW, United Kingdom; [b]Department of Ecology and Evolution, University of Lausanne, Lausanne CH-1015, Switzerland; [c]Department of Biology, Universidad Autónoma de Madrid, Madrid 28049, Spain; [d]Génomique Métabolique, Genoscope, Institut François Jacob, Commissariat à l'Énergie Atomique et aux Énergies Alternatives, CNRS, Université Evry, Université Paris-Saclay, Evry 91057, France; and [e]Genoscope, Institut François Jacob, Commissariat à l'Énergie Atomique et aux Énergies Alternatives, CNRS, Université Evry, Université Paris-Saclay, Evry 91057, France

1. D. Bachtrog *et al.*, Sex determination: Why so many ways of doing it? *PLoS Biol.* **12**, e1001899 (2014).
2. C. M. Disteche, Dosage compensation of the sex chromosomes. *Annu. Rev. Genet.* **46**, 537–560 (2012).
3. L. Gu, J. R. Walters, Evolution of sex chromosome dosage compensation in animals: A beautiful theory, undermined by facts and bedeviled by details. *Genome Biol. Evol.* **9**, 2461–2476 (2017).
4. J. E. Mank, Sex chromosome dosage compensation: Definitely not for everyone. *Trends Genet.* **29**, 677–683 (2013).
5. N. Brockdorff, B. M. Turner, Dosage compensation in mammals. *Cold Spring Harb. Perspect. Biol.* **7**, a019406 (2015).
6. R. Marin *et al.*, Convergent origination of a *Drosophila*-like dosage compensation mechanism in a reptile lineage. *Genome Res.* **27**, 1974–1987 (2017).
7. D. C. H. Metzger, B. A. Sandkam, I. Darolti, J. E. Mank, Rapid evolution of complete dosage compensation in poecilia. *Genome Biol. Evol.* **13**, evab155 (2021).
8. I. Darolti *et al.*, Extreme heterogeneity in sex chromosome differentiation and dosage compensation in livebearers. *Proc. Natl. Acad. Sci. U.S.A.* **116**, 19031–19036 (2019).
9. B. J. Meyer, Sex in the worm: Counting and compensating X-chromosome dose. *Trends Genet.* **16**, 247–253 (2000).
10. P. Chauhan *et al.*, Genome assembly, sex-biased gene expression and dosage compensation in the damselfly Ischnura elegans. *Genomics* **113**, 1828–1837 (2021).
11. D. J. Parker, K. S. Jaron, Z. Dumas, M. Robinson-Rechavi, T. Schwander, X chromosomes show relaxed selection and complete somatic dosage compensation across *Timema* stick insect species. *J. Evol. Biol.* **35**, 1734–1750 (2022).
12. A. Pal, B. Vicoso, The X Chromosome of Hemipteran insects: Conservation, dosage compensation and sex-biased expression. *Genome Biol. Evol.* **7**, 3259–3268 (2015).
13. J. G. Rayner, T. J. Hitchcock, N. W. Bailey, Variable dosage compensation is associated with female consequences of an X-linked, male-beneficial mutation. *Proc. Biol. Sci.* **288**, 20210355 (2021).
14. E. G. Prince, D. Kirkland, J. P. Demuth, Hyperexpression of the X chromosome in both sexes results in extensive female bias of X-linked genes in the flour beetle. *Genome Biol. Evol.* **2**, 336–346 (2010).
15. B. Vicoso, D. Bachtrog, Numerous transitions of sex chromosomes in Diptera. *PLoS Biol.* **13**, e1002078 (2015).
16. T. Conrad, A. Akhtar, Dosage compensation in *Drosophila melanogaster*: Epigenetic fine-tuning of chromosome-wide transcription. *Nat. Rev. Genet.* **13**, 123–134 (2012).
17. J. Djordjevic *et al.*, Dynamics of X chromosome hyper-expression and inactivation in male tissues during stick insect development. *PLoS Genet.* **21**, e1011615 (2025).
18. J. E. Mank, H. Ellegren, All dosage compensation is local: Gene-by-gene regulation of sex-biased expression on the chicken Z chromosome. *Heredity* **102**, 312–320 (2009).
19. P. S. Burgoyne, S. K. Mahadevaiah, J. M. A. Turner, The consequences of asynapsis for mammalian meiosis. *Nat. Rev. Genet.* **10**, 207–216 (2009).
20. B. D. McKee, M. A. Handel, Sex chromosomes, recombination, and chromatin conformation. *Chromosoma* **102**, 71–80 (1993).
21. A. I. Kalita, C. I. Keller Valsecchi, Dosage compensation in non-model insects–progress and perspectives. *Trends Genet.* **41**, 76–98 (2024).
22. J. B. Pease, M. W. Hahn, Sex chromosomes evolved from independent ancestral linkage groups in winged insects. *Mol. Biol. Evol.* **29**, 1645–1653 (2012).
23. F. N. Hamada, P. J. Park, P. R. Gordadze, M. I. Kuroda, Global regulation of X chromosomal genes by the MSL complex in *Drosophila melanogaster*. *Genes Dev.* **19**, 2289–2294 (2005).
24. T. Straub, G. D. Gilfillan, V. K. Maier, P. B. Becker, The *Drosophila* MSL complex activates the transcription of target genes. *Genes Dev.* **19**, 2284–2288 (2005).
25. A. I. Kalita *et al.*, The sex-specific factor SOA controls dosage compensation in *Anopheles* mosquitoes. *Nature* **623**, 175–182 (2023).
26. E. Krzywinska, P. Ribeca, L. Ferretti, A. Hammond, J. Krzywinski, A novel factor modulating X chromosome dosage compensation in *Anopheles*. *Curr. Biol.* **33**, 4697–4703.e4 (2023).
27. R. J. Davis, E. J. Belikoff, E. H. Scholl, F. Li, M. J. Scott, No blokes is essential for male viability and X chromosome gene expression in the Australian sheep blowfly. *Curr. Biol.* **28**, 1987–1992.e3 (2018).
28. M. A. Toups, B. Vicoso, Insect sex chromosome evolution: Conservation, turnover, and mechanisms of dosage compensation. *Curr. Opin. Insect Sci.* **72**, 101411 (2025).
29. N. Page *et al.*, Single-cell profiling of *Anopheles* gambiae spermatogenesis defines the onset of meiotic silencing and premeiotic overexpression of the X chromosome. *Commun. Biol.* **6**, 850 (2023).
30. S. Schoenmakers *et al.*, Female meiotic sex chromosome inactivation in chicken. *PLoS Genet.* **5**, e1000466 (2009).
31. S. H. Namekawa, J. T. Lee, XY and ZW: Is meiotic sex chromosome inactivation the rule in evolution? *PLoS Genet.* **5**, e1000493 (2009).
32. R. L. Kelley *et al.*, Expression of msl-2 causes assembly of dosage compensation regulators on the X chromosomes and female lethality in *Drosophila*. *Cell* **81**, 867–877 (1995).
33. M. A. Toups, B. Vicoso, The X chromosome of insects likely predates the origin of class Insecta. *Evolution* **77**, 2504–2511 (2023).
34. J. T. Lee, Disruption of imprinted X inactivation by parent-of-origin effects at Tsix. *Cell* **103**, 17–27 (2000).
35. C. J. van der Kooi, T. Schwander, On the fate of sexual traits under asexuality. *Biol. Rev. Camb. Philos. Soc.* **89**, 805–819 (2014).
36. J. M. Belote, J. C. Lucchesi, Control of X chromosome transcription by the maleless gene in *Drosophila*. *Nature* **285**, 573–575 (1980).
37. E. Lifschytz, D. L. Lindsley, The role of X-chromosome inactivation during spermatogenesis (*Drosophila*-allocycly-chromosome evolution-male sterility-dosage compensation). *Proc. Natl. Acad. Sci. U.S.A.* **69**, 182–186 (1972).
38. Z. Bao, A. Belyi, E. Argyridou, J. Parsch, Disruption of meiotic sex chromosome inactivation by X-autosome translocations in *Drosophila melanogaster*. *Genetics* **232**, iyag011 (2026).
39. C. C. Avelino *et al.*, Meiotic sex chromosome inactivation: Conservation across the *Drosophila* genus. *PLoS Genet.* **21**, e1011511 (2025).
40. T. Schwander, B. J. Crespi, Multiple direct transitions from sexual reproduction to apomictic parthenogenesis in *Timema* stick insects. *Evolution* **63**, 84–103 (2009).
41. T. Schwander, L. Henry, B. J. Crespi, Molecular evidence for ancient asexuality in *Timema* stick insects. *Curr. Biol.* **21**, 1129–1134 (2011).
42. J. Bast *et al.*, Consequences of asexuality in natural populations: Insights from stick insects. *Mol. Biol. Evol.* **35**, 1668–1677 (2018).
43. K. S. Jaron *et al.*, Convergent consequences of parthenogenesis on stick insect genomes. *Sci. Adv.* **8**, eabg3842 (2022).
44. Z. Dumas, W. Toubiana, M. Delattre, T. Schwander, Dynamics of recombination, X inactivation and centromere proteins during stick insect spermatogenesis. *PLoS Genet.* **21**, e1011827 (2025).
45. T. Schwander, B. J. Crespi, R. Gries, G. Gries, Neutral and selection-driven decay of sexual traits in asexual stick insects. *Proc. Biol. Sci.* **280**, 20130823 (2013).
46. S. Freitas, D. J. Parker, M. Labédan, Z. Dumas, T. Schwander, Evidence for cryptic sex in parthenogenetic stick insects of the genus Timema. *Proc. Biol. Sci.* **290**, 20230404 (2023).
47. S. Simon *et al.*, Old world and new world phasmatodea: Phylogenomics resolve the evolutionary history of stick and leaf insects. *Front. Ecol. Evol.* **7**, 345 (2019).
48. S. Bank, S. Bradler, A second view on the evolution of flight in stick and leaf insects (Phasmatodea). *BMC Ecol. Evol.* **22**, 62 (2022).
49. X. Li, J. E. Mank, L. Ban, The grasshopper genome reveals long-term gene content conservation of the X Chromosome and temporal variation in X Chromosome evolution. *Genome Res.* **34**, 997–1007 (2024).
50. Q.-L. Hu *et al.*, Chromosome-level assembly, dosage compensation and sex-biased gene expression in the small brown planthopper, Laodelphax striatellus. *Genome Biol. Evol.* **14**, evac160 (2022).
51. A. M. Rice, Y. Li, P. Donnelly, A. McLysaght, Evolution of dosage-sensitive genes by tissue-restricted expression changes. *Genome Biol. Evol.* **17**, evaf132 (2025).
52. J. Larsson, M. J. Svensson, P. Stenberg, M. Mäkitalo, Painting of fourth in genus *Drosophila* suggests autosome-specific gene regulation. *Proc. Natl. Acad. Sci. U.S.A.* **101**, 9728–9733 (2004).
53. J. E. Mank, D. J. Hosken, N. Wedell, Some inconvenient truths about sex chromosome dosage compensation and the potential role of sexual conflict. *Evolution* **65**, 2133–2144 (2011).
54. E. Flintham, V. Savolainen, S. P. Otto, M. Reuter, C. Mullon, The maintenance of genetic polymorphism underlying sexually antagonistic traits. *Evol. Lett.* **9**, 259–272 (2025).
55. D. C. Lahti *et al.*, Relaxed selection in the wild. *Trends Ecol. Evol.* **24**, 487–496 (2009).
56. D. J. Futuyma, Evolutionary constraint and ecological consequences. *Evolution* **64**, 1865–1884 (2010).
57. H. Defendini *et al.*, The release of sexual conflict after sex loss is associated with evolutionary changes in gene expression. *Proc. Biol. Sci.* **292**, 20242631 (2025).
58. S. Koren *et al.*, Canu: Scalable and accurate long-read assembly via adaptive k-mer weighting and repeat separation. *Genome Res.* **27**, 722–736 (2017).
59. M. Kolmogorov, J. Yuan, Y. Lin, P. A. Pevzner, Assembly of long, error-prone reads using repeat graphs. *Nat. Biotechnol.* **37**, 540–546 (2019).
60. H. Li, Minimap2: Pairwise alignment for nucleotide sequences. *Bioinformatics* **34**, 3094–3100 (2018).
61. R. Vaser, I. Sović, N. Nagarajan, M. Šikić, Fast and accurate de novo genome assembly from long uncorrected reads. *Genome Res.* **27**, 737–746 (2017).
62. H. Li, Aligning sequence reads, clone sequences and assembly contigs with BWA-MEM. arXiv [Preprint] (2013). https://doi.org/10.48550/arXiv.1303.3997 (Accessed 29 June 2026).
63. B. J. Walker *et al.*, Pilon: An integrated tool for comprehensive microbial variant detection and genome assembly improvement. *PLoS One* **9**, e112963 (2014).
64. D. R. Laetsch, M. L. Blaxter, BlobTools: Interrogation of genome assemblies. *F1000Research* **6**, 1287 (2017).
65. M. J. Roach, S. A. Schmidt, A. R. Borneman, Purge haplotigs: Allelic contig reassignment for third-gen diploid genome assemblies. *BMC Bioinformatics* **19**, 460 (2018).
66. N. C. Durand *et al.*, Juicer provides a one-click system for analyzing loop-resolution Hi-C experiments. *Cell Syst.* **3**, 95–98 (2016).
67. O. Dudchenko *et al.*, De novo assembly of the *Aedes aegypti* genome using Hi-C yields chromosome-length scaffolds. *Science* **356**, 92–95 (2017).
68. M. Seppey, M. Manni, E. M. Zdobnov, BUSCO: Assessing genome assembly and annotation completeness. *Methods Mol. Biol.* **1962**, 227–245 (2019).
69. T. Brůna, K. J. Hoff, A. Lomsadze, M. Stanke, M. Borodovsky, BRAKER2: Automatic eukaryotic genome annotation with GeneMark-EP+ and AUGUSTUS supported by a protein database. *NAR Genom. Bioinform.* **3**, lqaa108 (2021).

70. J. M. Flynn *et al.*, RepeatModeler2 for automated genomic discovery of transposable element families. *Proc. Natl. Acad. Sci. U.S.A.* **117**, 9451–9457 (2020).
71. A. Smith, R. Hubley, P. Green, RepeatMasker Open-4.0. (2013). http://www.repeatmasker.org.
72. E. V. Kriventseva *et al.*, OrthoDB v10: Sampling the diversity of animal, plant, fungal, protist, bacterial and viral genomes for evolutionary and functional annotations of orthologs. *Nucleic Acids Res.* **47**, D807–D811 (2019).
73. D. J. Parker, J. Djordjevic, T. Schwander, Olfactory proteins in *Timema* stick insects. *Front. Ecol. Evol.* **7**, 101 (2019).
74. A. M. Bolger, M. Lohse, B. Usadel, Trimmomatic: A flexible trimmer for Illumina sequence data. *Bioinformatics* **30**, 2114–2120 (2014).
75. A. Dobin *et al.*, STAR: Ultrafast universal RNA-seq aligner. *Bioinformatics* **29**, 15–21 (2013).
76. M. Stanke *et al.*, AUGUSTUS: Ab initio prediction of alternative transcripts. *Nucleic Acids Res.* **34**, W435–W439 (2006).
77. T. Brůna, A. Lomsadze, M. Borodovsky, Genemark-EP+: Eukaryotic gene prediction with self-training in the space of genes and proteins. *NAR Genom. Bioinform.* **2**, lqaa026 (2020).
78. E. P. Nawrocki, S. R. Eddy, Infernal 1.1: 100-fold faster RNA homology searches. *Bioinformatics* **29**, 2933–2935 (2013).
79. D. M. Emms, S. Kelly, OrthoFinder: Phylogenetic orthology inference for comparative genomics. *Genome Biol.* **20**, 238 (2019).
80. A. R. Quinlan, I. M. Hall, BEDTools: A flexible suite of utilities for comparing genomic features. *Bioinformatics* **26**, 841–842 (2010).
81. C. Larose, G. Lavanchy, S. Freitas, D. J. Parker, T. Schwander, Facultative parthenogenesis: A transient state in transitions between sex and obligate asexuality in stick insects? *Peer Community J.* **3**, e60 (2023).
82. S. Anders, P. T. Pyl, W. Huber, HTSeq–A Python framework to work with high-throughput sequencing data. *Bioinformatics* **31**, 166–169 (2015).
83. M. D. Robinson, D. J. McCarthy, G. K. Smyth, edgeR: A Bioconductor package for differential expression analysis of digital gene expression data. *Bioinformatics* **26**, 139–140 (2010).
84. Y. Benjamini, Y. Hochberg, Controlling the false discovery rate: A practical and powerful approach to multiple testing. *J. R. Stat. Soc. Ser. B Stat. Methodol.* **57**, 289–300 (1995).
85. W. Toubiana, T. Schwander, Timema cristinae isolate WT-2025d, whole genome shotgun sequencing project. GenBank. https://www.ncbi.nlm.nih.gov/nuccore/JBOIUC000000000.1/. Deposited 28 May 2025.
86. D. J. Parker *et al.*, Timema podura isolate WT-2025b, whole genome shotgun sequencing project. GenBank. https://www.ncbi.nlm.nih.gov/nuccore/JBOIUD000000000. Deposited 28 May 2025.
87. D. J. Parker *et al.*, Sequencing data for the stick insect Timema podura: ONT and Illumina reads. National Center for Biotechnology Information Sequence Read Archive. https://www.ncbi.nlm.nih.gov/bioproject/PRJEB94285. Deposited 25 July 2025.
88. D. J. Parker *et al.*, Timema species genomic sequencing. National Center for Biotechnology Information Sequence Read Archive. https://www.ncbi.nlm.nih.gov/bioproject/PRJNA1293928. Deposited 21 July 2025.
89. D. J. Parker *et al.*, Timema cristinae and Timema monikense raw RNAseq sequence reads. National Center for Biotechnology Information Sequence Read Archive. https://www.ncbi.nlm.nih.gov/bioproject/PRJNA1320679. Deposited 5 September 2025.
90. D. J. Parker *et al.*, Timema podura and Timema genevievae RNAseq. National Center for Biotechnology Information Sequence Read Archive. https://www.ncbi.nlm.nih.gov/bioproject/PRJNA1327219. Deposited 11 September 2025.
91. D. J. Parker, Archived code repository. Zenodo. https://doi.org/10.5281/zenodo.21038455. Deposited 29 June 2026.